NASA CR-54406
Series 6, Issue 34

QUARTERLY PROGRESS REPORT:

INVESTIGATION OF KILOVOLT ION SPUTTERING

by

HAROLD P. SMITH, JR., F. C. HURLBUT AND T. H. PIGFORD

prepared for

NATIONAL AERONAUTICS AND SPACE ADMINISTRATION

CONTRACT NAS 3-5743

SPACE SCIENCES LABORATORY
UNIVERSITY OF CALIFORNIA, BERKELEY

NASA CR-54406
Series 6, Issue 34

QUARTERLY PROGRESS REPORT:

INVESTIGATION OF KILOVOLT ION SPUTTERING

by

Harold P. Smith, Jr., F. C. Hurlbut, and T. H. Pigford

prepared for

NATIONAL AERONAUTICS AND SPACE ADMINISTRATION

July 31, 1965

CONTRACT NAS 3-5743

Technical Management
NASA Lewis Research Center
Cleveland, Ohio

Electric Propulsion Office
Mr. J. A. Wolters

SPACE SCIENCES LABORATORY
University of California, Berkeley 94720

TABLE OF CONTENTS

FIGURES:

FIGURES (continued)

Fig. 5A. Angular distribution normalized to isotropic emission for cesium ion sputtering of monocrystalline copper. The 1.0 KeV ion beam was 45 degrees from the surface normal and parallel to the ⟨110⟩ vector. The angular position of each point is depicted in Fig. 4.

Fig. 5B. Angular distribution normalized to isotropic emission for cesium ion sputtering of monocrystalline copper. The 2.5 KeV ion beam was 45 degrees from the surface normal and parallel to the ⟨110⟩ vector. The angular position of each point is depicted in Fig. 4.

Fig. 5C. Angular distribution normalized to isotropic emission for cesium ion sputtering of monocrystalline copper. The 5.0 KeV ion beam was 45 degrees from the surface normal and parallel to the ⟨110⟩ vector. The angular position of each point is depicted in Fig. 4.

Fig. 5D. Angular distribution normalized to isotropic emission for cesium ion sputtering of monocrystalline copper. The 7.5 KeV ion beam was 45 degrees from the surface normal and parallel to the ⟨110⟩ vector. The angular position of each point is depicted in Fig. 4.

Fig. 5E. Angular distribution normalized to isotropic emission for cesium ion sputtering of monocrystalline copper. The 10.0 KeV ion beam was 45 degrees from the surface normal and parallel to the ⟨110⟩ vector. The angular position of each point is depicted in Fig. 4.

Fig. 6A. Angular distribution normalized to isotropic emission for cesium ion sputtering of monocrystalline copper. The 1.0 KeV ion beam was 45 degrees from the surface normal and parallel to the ⟨557⟩ vector. The angular position of each point is depicted in Fig. 4.

Fig. 6B. Angular distribution normalized to isotropic emission for cesium ion sputtering of monocrystalline copper. The 2.5 KeV ion beam was 45 degrees from the surface normal and parallel to the ⟨557⟩ vector. The angular position of each point is depicted in Fig. 4.

Fig. 6C. Angular distribution normalized to isotropic emission for cesium ion sputtering of monocrystalline copper. The 7.5 KeV ion beam was 45 degrees from the surface normal and parallel to the ⟨557⟩ vector. The angular position of each point is depicted in Fig. 4.

FIGURES (continued)

Fig. 7. Schematic diagram of proton induced characteristic x-ray detection system.

Fig. 8. Residual areal density of implanted ions, F (ions/cm^2), as a function of the depth of erosion, D (cm). The parameters are plotted as dimensionless groups according to the relationship shown in Eq (12). A linear approximation to the exact solution is depicted.

Fig. 9. Saturation areal ion density, I_{T^∞} (ions/cm^2) as a function of the sputtering yield, ion penetration range, and ion straggling. The parameters are plotted as dimensionless groups according to the relationship shown in Eq (14). Two limiting cases are also depicted.

TABLES:

1. Relative angular distribution normalized to isotropic emission as a function of ion energy for normal bombardment of the (100) plane with the target temperature equal to 87°K. The angular position number corresponds to that shown in Fig. 3. Azimuthal orientation of the (010) plane which contains a ⟨110⟩ closepacked vector is shown for each measurement.

2. Relative angular distribution at 473°K. The bombardment conditions and configuration are analogous to those presented in Table 1.

QUARTERLY PROGRESS REPORT:

INVESTIGATION OF KILOVOLT ION SPUTTERING

by

Harold P. Smith, Jr., F. C. Hurlbut, and T. H. Pigford
Space Sciences Laboratory, University of California, Berkeley

ABSTRACT

Investigation of cesium ion sputtering of monocrystalline copper using a radioactive tracer technique has continued. During the past quarter, the yield and angular distribution of sputtered copper has been measured as a function of cesium ion energy variation from 1 to 10 KeV for the following cases: (a) ion beam parallel to the surface normal and to the ⟨100⟩ crystallographic vector with the target at 87 and 473 degrees K., (b) ion beam rotated 45 degrees from the surface normal and parallel to the ⟨110⟩ vector, and (c) ion beam again 45 degrees from the surface normal but parallel to the ⟨557⟩ vector. It was found that temperature variation had little effect, but that alignment of the beam parallel to a high (Miller) index direction greatly enhanced the yield. The angular data has been successfully fitted to an analytic function through use of a non-linear regression analysis. This method will be used to describe the effects of the above parameters on the angular distribution.

Further progress in the development of a mercury ion sputtering apparatus and in a time-of-flight velocity spectrum technique is presented, as well as initial work in developing a technique for measuring small surface densities through use of proton induced characteristic x-rays.

Finally, a project to study saturated ion implantation distributions has been initiated. An analysis of expected distributions using a linear model of the combined implantation-sputtering phenomena is presented.

Author

INTRODUCTION

Sputtering or ionic erosion of the accel electrode and focusing structure of the ion rocket engine can be the dominant mechanism limiting long term operation of the engine. Although the field of sputtering has been known since the phenomenon of gas discharge was first observed, no reliable theory to predict the yield, angular distribution, and velocity spectrum has been developed. Furthermore, it has only been within the past few years that experiments have been made under suitably defined conditions. In addition, there has been little work with either cesium or mercury beams so that it is difficult to predict the electrode erosion on the basis of previous data. For these reasons, the Lewis Research Center has sponsored detailed investigation of the sputtering of copper and molybdenum crystals under cesium and mercury ion beam bombardment where the target parameters such as temperature, angle of incidence, etc., are well known and varied over the range of interest.

The University of California (Berkeley) Space Sciences Laboratory began an investigation of this field early in 1964. Five vacuum systems have been constructed to study these effects using radioactive tracer techniques and activation analysis to measure the yield and angular distribution and mass spectrographic and time-of-flight analysis to determine the velocity spectrum of the various sputtered particles. Additional work has recently been initiated to study the saturation distribution of bombardment ions in the target lattice and to develop a method for measuring fractional monolayer surface densities through detection of proton induced characteristic x-rays.

This document is submitted as a progress report on our continuing

effort to develop suitable and versatile apparata for measurement of these phenomena.

I. Cesium Ion Sputtering*

The measurements of cesium ion sputtering of copper reported in the last progress report and presented at the recent San Francisco meeting of the AIAA,[1] have been extended during the past quarter to measurement of the yield and angular distribution for normal bombardment of the (100) crystallographic face with the target temperature at 87°K and at 473°K. In addition, similar measurements have been made for non-normal bombardment in which the angle between the cesium ion beam and the surface normal was 45°. Two series of measurements were made. One with the beam parallel to the ‹110› crystallographic direction in the lattice, and the second with the beam parallel to the ‹557› direction (i. e., The ion beam was not parallel to any low index crystallographic direction). The yields for these latter measurements are greatly enhanced over those encountered with the beam parallel to low index directions. The sputtering yield for these measurements is shown in Figs. 1 and 2. The angular distribution normalized to isotropic emission for normal bombardment are presented in Tables 1 and 2 in which the angular position may be determined by reference to Fig. 3. The angular distribution for runs made with the beam 45° from the surface normal are shown in Figs. 5 and 6.

Discussion of these results will be postponed until the data has been subjected to a non-linear regression analysis. Preliminary results using this technique are presented below and will be extended to the complete array of data during the next quarter.

---

*The work reported in this section was performed by N. Thomas Olson and Harold P. Smith, Jr.

It is assumed that the angular distribution results from two phenomena which can be superimposed. The first is associated with Lambert's law of emission which would apply exactly in the case of isotropic scattering in the laboratory system of randomly placed particles in the surface. This type of emission follows a cosine distribution about the polar angle measured from the surface normal. The second phenomenon considers the lattice structure. In particular, preferred emission in the form of gaussian peaks is assumed in the closed-packed ⟨110⟩ and ⟨100⟩ directions. We have not yet decided how to propose a function to fit the {111} planar emission which has been simulated by Professor D. E. Harrison, Jr.[3] and has been observed by us and by other experimenters as noted in the previous progress report.[2] As a result of these assumptions, it is assumed that the angular distribution of sputtered particles can be represented by the following function.

$$S(\theta,\varphi) = a_1 \cos\theta + a_2 \exp\left\{-(\theta-\theta_1)^2/2\sigma_1^2\right\} \exp\left\{-(\varphi-\varphi_1)^2 \sin^2\theta_1/2\sigma_1^2\right\} + a_3 e^{-\theta^2/2\sigma_2^2} \quad (1$$

where

$S(\theta,\varphi)$ = atoms/ion sr

θ = polar angle measured from the surface normal

θ_1 = polar angle of the ⟨110⟩ vector

φ_1 = azimuthal angle of the ⟨110⟩ vector

a_1, a_2, a_3, σ_1, σ_2 = fitting parameters

Use of this equation is restricted to those experiments made under normal bombardment but extension of this type of fitting function to non-normal

bombardment is straightforward. In final operation, the 100 angular distribution data points are supplied to the non-linear regression program. A high-speed digital computer then calculates the best values (based on a least mean square error criterion) of fitting parameters a_1, a_2, a_3, σ_1, and σ_2. It appears that the use of this type of data reduction and presentation provides the best means for discussing the voluminous amount of data that is generated by the technique described previously.[1, 2]

As a preliminary attempt to apply non-linear regression analysis, we have chosen the 17 data points that represent the angular emission in the two (100) planes that intercept the (100) surface plane. These data were then fitted to the following reduced fitting function,

$$S(\theta) = a_1 \cos\theta + a_2 \exp\left\{-(\theta - \pi/4)^2/2\sigma_1^2\right\} \qquad (2$$

in which there are only three fitting parameters a_1, a_2, and σ_1. The computer calculation was then able to provide values for the fitting parameters such that the average deviation of the data points from the Eq. (2) was less than 7%. Since over 17 data points are considered by only three fitting constants, the small deviation is encouraging and indicates that the technique will be a suitable method for discussing the angular distribution data.

Assuming that the fitting function suggested above satisfactorily fits the angular data, then one can integrate the angular emission function over the solid angle in order to determine the intensities of cosinusoidal emission and the gaussian emission which is based on crystal lattice structure and to some extent on the concept of focused collision chains leading to a sputtering event. The results of integration are shown below where S_{cos} refers to Lambert Law emission, S_{110} refers to emission in the most closed pack direction and finally S_{110} refers to emission in the $\langle 100 \rangle$ direction.

$$\frac{S_{cos}}{S} = \frac{\pi a_1}{S}$$

$$\frac{S_{110}}{S} = \frac{8\pi a_2 \sigma_1^2}{S} \qquad (3$$

$$\frac{S_{100}}{S} = \frac{2\pi a_3 \sigma_2^2}{S}$$

Application of Eq. (3) to the results based on the fitting function shown in Eq. (2) indicated that 44% of the emitted particles can be associated with the cosine distribution; the remaining particles are emitted in the $\langle 110 \rangle$ gaussian distribution. Although these results are preliminary and do not merit extensive discussion, it appears that the exclusive use of focused emission principles in discussing the phenomenon of sputtering has been over-emphasized in the recent literature since our results indicate that almost half of the particles can be associated with a Lambert Law type of emission. This part of the angular distribution can then be associated with a local thermal heating model of the surface similar to that proposed by Charles Townes two decades ago.[4]

Our measurements of cesium copper sputtering have now been essentially completed. In the coming quarter we will extend this type of investigation to cesium molybdenum sputtering. However, these measurements will be postponed as a result of a decision to measure first cesium-aluminum sputtering under the good vacuum conditions inherent in this particular apparatus.

II. Mercury Ion Sputtering*

Construction and assembly of apparatus for mercury ion sputtering

---

*The work reported in this section was performed by R. G. Musket.

similar to that used with cesium is continuing. This apparatus is of necessity more complex as a result of the formation of multiply charged mercury ions in the electron bombardment ion source. In order to insure that only singly charged (or only doubly charged) mercury ions of known energy strike the target, it is necessary to pass the ion beam through the bending magnet. Following successful transport and analysis of the mercury ion beam, sputtering measurements on copper and molybdenum are easily made in a manner analogous to that used for cesium-copper sputtering.[1, 2]

The mercury ion source continues to operate in an acceptable and reproducible manner. We find that the source can be cycled between ambient pressure and vacuum without adverse affect. Steady operation for periods over an hour seems to offer no difficulty indicating that thermal regulation of the mercury reservoir by simple thermal conductivity is satisfactory. No oscillations have been noticed in the plasma discharge.

Two overlapping einsel lenses satisfactorily transport the beam over a distance of four inches and reform the beam from its slit geometry at the source exit to a circular geometry near the magnet entrance. Similar einsel lens designs have been tested for transmission both to and from the magnet chamber. Transmissions of .96/in. have been measured at a total current of 250 μa through a 1/2 inch diameter lens aperture. The source and its associated lens system have been found to operate most satisfactorily at 10 KV, and we are currently considering continuous source operation at this voltage and obtaining ion energy variation through an isolated, variable potential target.

Construction of the final target, magnet, and source chambers has

been completed. Full system operation and preliminary measurements are planned for the coming quarter.

III. Velocity Spectrum Measurement*

In performing an analysis of the velocity spectrum of sputtered particles, the parent ion beam is first modulated by electrostatic techniques and then allowed to impinge on a target as a series of discrete pulses. Since the time lapse in sputtering is of negligible magnitude in comparison with flight times of the sputtered particles and since the ion flight time from modulator to target is known, spectra of arrival times of sputtered particles on a detector are immediately translatable into spectra of velocities for those particles. Analysis proceeds straightforwardly if the parent ion beam is monoenergetic. The elements of an arrival time analysis system are modulated ion source, ionizer, spectrometer, multiplier detector, signal amplifier train, data acquisition system. Progress in the last quarter in the development and testing of each of these system elements is indicated below.

The ion source in this experiment is a cesium surface contact ionization type. During the past quarter the electrostatic deflection modulator has been replaced by transmission barrier which has been found successfully to transmit 60% of the ions in the open condition and to stop all but 0.2% in the shutoff condition. This technique has the advantage over the deflection system of reducing the voltage wave requirements on the electronic pulse assembly since any voltage above the source voltage is capable of stopping the beam whereas an accurate square wave pulse is

---

*Work reported in this section was performed by D. W. DeMichele, F. C. Hurlbut, and Harold P. Smith, Jr.

necessary in the beam deflection system. Although the modulator network seems to be working acceptably, difficulty was encountered in actual source operation. This trouble seems to ensue from a poor cesium reservoir seal which allowed cesium to coat a number of surfaces and in some cases greatly increased electron flow within the source assembly. Finally testing was interrupted as a result of a break in the ionizer heater circuit. The source heater and reservoir seal are currently under repair; continued operation following repair is expected early in the next quarter.

A new ionizer and multiplier detector have been added to the mass spectrometer system. These elements appear to be operating perfectly and reproducibly. Since these elements are under vacuum almost all the time no problems are envisioned in their continued operation.

Further improvements have been made to the ultrahigh vacuum system in which the experiment will be performed. An internal cryogenic reservoir-pump has been added and found to reduce the system pressure by an order of magnitude. In addition, quartz rod heaters have been installed to assist in vacuum system bakeouts.

Preliminary measurements have been made to investigate coupling between the modulated ion source and mass spectrometer systems. These investigations show the mass spectra in the mass range 60-70 with the ion source operating at high voltage, without high voltage, and with source heater off. The mass peaks associated with source operation in the mass range of copper is cause for concern, however, bakeout above 200°C has not yet been attempted and may remove the mass peaks in the 60-70 range since they are probably associated with hydrocarbon contamination of the source.

Electron flow between the ion source and the mass spectrometer ionizer can be detected. Shielding for both these systems is currently being constructed. Furthermore, the shield about the cesium ion source will be cooled in order to provide additional surfaces for adsorbing free cesium, thereby prolonging the life of the vacuum ion pump. A final coupling problem may result from simultaneous operation of the ion beam pulser in conjunction with the mass spectrometer multiplier detector system. However, this coupling should not be serious since the arrival of the sputtered particles at the detector follows the ion beam pulse. Hence, simple gating circuitry on the scalers should guard against this coupling if present.

An improved preamplifier mounted directly to the multiplier output has been installed and tested. In addition, further shielding against the RF pickup of the quadrapole field in the multiplier circuit has been installed. The preamplifier converts the pulse of single ion induced electrons from the multiplier output to a 100-500 mV pulse with rise time less than 10 nsec and full width at half maximum of 20 nsec. These pulses are more than adequate for high-speed scaling. No problem is envisioned in this particular phase of the program. The necessary high-speed scalers have been delivered. Finally, a second electronic high voltage pulser has been constructed and has found to be superior to the initial pulser. It is hoped that this second pulser will be satisfactory for use in a deflection system and may offer less coupling to the multiplier.

IV. Aluminum Sputtering*

A preliminary measurement of the sputtering yield of 2.5 Kev cesium ions bombarding monocrystalline aluminum has been made in the

---

*Work in this section was performed by A. E. Andrews and E. H. Hasseltine.

apparatus described in Reference 2. During the experiment the pressure was maintained at 1×10^{-7} torr and the sputtered aluminum was collected on 1 mil high purity lead foil as described in the previous progress report. The ion current to the .3 cm^2 target was between 20-25 μa. This yields a ratio of contaminant flux to the target divided by sputtered particle flux from the target of less than 0.1. Hence it can be assumed that bombardment took place under clean surface conditions. The experiment continued until 46 millicoulombs were deposited on the target. Following sputtering, the collector was analyzed for aluminum by neutron activation analysis of the foil as described in Reference 2. A 7.5 minute irradiation was performed at the LPTR (Livermore Pool Type Reactor); the sputtering yield in this case was measured at 1.95 atoms/ion. During the experiment the ion beam was normal to the aluminum surface and within 5^o of the $\langle 110 \rangle$ crystallographic vector of the face centered cubic, aluminum lattice.

Immediately following this initial measurement, the apparatus needed for these measurements became unavailable as a result of a higher priority assigned to the cesium-copper sputtering measurements. An additional system employing apparatus already available within the laboratory was undertaken. An einsel lens system was mounted on a conventional cesium ion source, and the entire assembly was placed in a glass vacuum system utilizing an oil diffusion pump and cryogenic baffle which maintained a pressure during bombardment of 2×10^{-6} torr. This system produced a highly collimated, small divergence cesium ion beam with a current density of 20 microamps/cm^2 at the target. The energy of the ions could be varied from 1-10 Kev. In this case, the ratio of contaminant flux to sputtered flux is of the order of unity. Residual gas analysis by a mass spectrometer of

the vacuum system shows that 20% of the contaminant flux can be associated with oxygen. Hence, there is a strong probability that sputtering in this chamber would take place in the presence of a complete or partial film of aluminum oxide on the target. This condition is not satisfactory for well defined measurements of cesium-aluminum sputtering.

As noted in Section I of this report, our measurements of cesium-copper sputtering are essentially completed, therefore, this apparatus, which is capable of maintaining lower pressures than that noted above, can be used for the cesium-aluminum sputtering. In this chamber sputtering takes place under clean surface conditions; furthermore, the reliability of the measurements can be enhanced by employing our mass spectrometer to monitor the vacuum system residual gases during the sputtering processes. Actual measurements will be made early in the coming quarter. Some consideration is being given to the possibility of constructing an additional small ultrahigh vacuum chamber for the aluminum and the alumina measurements in order to reduce the work load on this apparatus.

Preliminary planning is now under way for measurement of the angular distribution of sputtered alumina using an electron microprobe recently purchased by the University of California. This instrument should represent an ideal manner for obtaining the angular data without recourse to enumerable irradiations necessary in neutron activation analysis of sputtering aluminum.

V. Surface Density Measurements*

The objective of the surface density program is to measure (in ultrahigh vacuum) the surface atom density of oxygen adsorbed on an alumi-

---

*Work reported in this section was performed by R. R. Hart, G. K. Cowell, J. M. Kahn, and Harold P. Smith, Jr.

num substrate. This is to be accomplished by detecting and counting characteristic oxygen and aluminum x-rays induced in the surface by magnetically analyzed 100 KeV proton beam from a duoplasmatron ion source. The x-rays are to be detected and scaled using gas flow proportional counter techniques.

Bids have been received from various manufacturers for all major equipment required. The purchase of this equipment is awaiting NASA approval but is expected to be completed in early August. All items should be received within six weeks of purchase date with the possible exception of the ultrahigh vacuum target chamber.

A 6" cryogenically baffled 1500 l/sec diffusion pump system to be used in conjunction with the duoplasmatron ion source has been assembled and tested. A pressure of 2×10^{-7} torr was obtained without bakeout in a blanked pyrex glass cross. Since the ion source is expected to operate in the 10^{-6} torr pressure range, this pumping system should be adequate.

A double window gas flow x-ray proportional counter together with an x-ray absorbing chamber has been designed and constructed as shown in Fig. 7. Two primary development objectives have been (a) to construct an x-ray window which will transmit the low energy (23.7 Å) characteristic oxygen x-ray but still have sufficient strength to withstand between 10 and 50 torr proportional counter gas pressure, and (b) to provide an ultrahigh vacuum seal which will not interfere with x-ray transmission. The first problem was solved by using Al_2O_3 windows which can be made thick enough to withstand the required pressure but still transmit the oxygen x-ray due to the low mass absorption cross section (3276 cm^2/g)[5]. The second problem was solved by using a 0.0015 in. thick aluminum foil

gasket as an ultrahigh vacuum seal with the alumina window as the center of the gasket. Use of the window-aluminum assembly also enables bakeout of the ultrahigh vacuum system.

The combination window-gasket assembly has been successfully prepared with window thickness from 1000 - 4000 Å, corresponding to characteristics of oxygen x-ray transmission coefficients of 0.88-0.59. The procedure followed is similar to that given by Harris[6]. Essentially, the method consists of anodizing both surfaces of an aluminum foil in a 3% ammonium tartrate solution at a pre-determined voltage for a given length of time. Aluminum oxide layers, whose thickness depends on the voltage, are formed on each side of the aluminum foil. Sodium hydroxide is then applied to the center area of one surface of the anodized foil and dissolves the Al_2O_3 on that area, thus exposing but not dissolving the underlying aluminum. The center section of a foil is then immersed in hydrochloric acid which dissolves the exposed aluminum but does not attack the alumina. The final result is then a thin alumina window in the center of an anodized aluminum foil. We have found that these window-gasket foils rarely rupture during installation. Further work will include testing for possible permeability of the window to counter gas and determining maximum gas pressure before window rupture.

A second window (aluminum foil only) on the proportional counter is intended to minimize background noise resulting from secondary electron emission caused by the relatively high energy characteristic aluminum x-rays (8.3 Å) which impinge on the far wall of the counter. A 38,000 Å aluminum window will allow 72% of these x-rays to leave the counter without photoelectric interaction. An additional chamber at forepump pressure

can be added beyond this window if necessary to prevent window rupture by atmospheric pressure. Furthermore, this additional chamber can serve as a proportional counter for detecting Al x-rays.

An additional chamber upstream from the proportional counter is included in the design in order to facilitate placement of absorber foils in the path of the x-ray beam. Incorporation of these foils then allows selective transmission of the various characteristic x-rays; thus enhancing the versatility and sensitivity of the counter system.

VI. Investigation of Heavy Ion Penetration*

A necessary first step in the detailed understanding of the sputtering process is the investigation of the eventual distribution of bombardment ions in the solid lattice. As a result of this, an experimental study of ion penetration has been initiated during the past quarter. The existing literature concerning theoretical and experimental investigation of penetration of ions has been collected and carefully reviewed. The measurements to be described below are a logical extension of the experimental study of ion penetration by J. A. Davies et al.[7] Their work as well as computer simulation of the phenomenon by Robinson and Oen[8, 9] was restricted to measurement or simulation of very light bombardment conditions. Our measurements will attempt to extend their techniques to the heavy ion bombardment conditions that exist in ion rocket electrode sputtering. With exception to the work by Brown and Davies[10] very little work has been done in this area. There has been essentially no theoretical treatment of the non-linear ion penetration effect where the nonlinearity arises from ion-ion collisions within the lattice.

---

*The work reported in this section was performed by W. F. J. Siekhaus, T. H. Pigford, and Harold P. Smith, Jr.

The proposed experiment is based on the detection of cesium and mercury ions (or atoms) by neutron activation following bombardment as opposed to the techniques of J. A. Davies which utilized radioactive tracer ion bombardment. Both mercury and cesium have long half-life gamma emitting isotopes (Hg 203: $T_{1/2}$ = 47 days and cesium 134: $T_{1/2}$ = 2.1 years). Hence, activation of the bombarded aluminum and copper lattices and low background counting following decay of the short-lived aluminum and copper activation isotopes is suitable for determining the absolute amount of cesium or mercury in the lattice. Conservative calculations show that this technique should be sufficiently sensitive to measure 10^{13} atoms of mercury or cesium. Since quantities of this magnitude are deposited by a microcoulomb of ion bombardment, target activation after bombardment is acceptable. The spatial distribution is determined by alternating a selective target surface stripping technique with gamma detection of the residual cesium or mercury. The necessary low background shield or counter for this work has been assembled and tested. Calibration will be carried out during the coming quarter.

Attention has been given to the question of saturation; i. e., to the maximum areal density of ions that can be implanted in a material. It is shown in the next section that this number should be proportional to the mean depth of penetration and inversely proportional to the sputtering yield. Incorporation of these parameters for the experiments noted above shows that over 10^{15} atoms/cm^2 can be implanted at saturation.

The contract calls for investigation of penetration depth as a function of various crystallographic directions. Hence, accurate (small divergence) beam alignment is necessary. A cylindrical lens system has

been constructed to provide a dense parallel beam of cesium ions downstream from a circular surface ionization cesium source. The lens was designed with a long focal length and the target was mounted just in front of the focusing point of the beam. The angular divergence of the beam at the target should be less than 5^{o}. In order to adjust for small deviations of the beam from the cylindrical axis a dual pair of deflection plates is now under construction and will be installed immediately downstream from the extractor plate.

The source-lens-target assembly is mounted in a glass vacuum system with a pressure of the order of 10^{-7} torr. Since current densities of the order of or greater than 100 $\mu a/cm^2$ should be attainable, the bombardment should take place under clean surface conditions. However, the initial tests of the bombardment system have not yielded a sufficiently high current density. This seems to result from misalignment which can be corrected following installation of the dual deflection plates. As soon as a sufficiently dense ion beam has been attained a saturation bombardment of cesium on aluminum will be made and the distribution of cesium will be measured as discussed above.

The stripping technique is analogous to that discussed in the preceding section to form thin windows of Al_2O_3. This technique is well documented and no problems are envisioned in this particular phase of the measurement.

VII. Saturation Distribution of Implanted Ions*

Introduction

High energy ion bombardment of a solid surface results in the entrapment or implantation of the ion species in the first few layers of the

---

*The work reported in this section was performed by Harold P. Smith, Jr.

solid material.[7, 11, 12, 13, 14] Concomitantly, the ion bombardment removes a small amount of the surface through the sputtering process.[15] These competing effects eventually result in a saturation distribution of the implanted ions within the latice.[16] Although a detailed understanding of this process is of fundamental importance in the investigation of radiation damage and sputtering, an added impetus for a study of ion implantation is the scope of its technological applications. As a primary example, sensitive investigation of surface erosion can be accomplished by entrapment of krypton-85, a radioactive tracer, in selected critical areas of the surface to be studied. Reduction in the in situ gamma ray count rate during the erosion process then provides a continuous and sensitive measure of erosion to a depth comparable to the mean distance of ion penetration.

An approximate model of the competing processes of implantation and sputtering is presented in this paper as an attempt to provide a simple procedure for calculation of the condition necessary for saturation, the maximum areal density of implanted ions, and the residual activity remaining as the erosion process proceeds. It is assumed that (a) the bombardment ions interact only with an undamaged lattice and (b) the entrapped ions remain immobile until the material in which they reside is removed by sputtering. The model is similar to that of Carter, Colligon, and Leck[16] but extends their treatment to explicit calculations and differs in the condition required for saturation.

The most serious approximation inherent in the model is the neglect of ion-ion collisions which occur with high probability at saturation. The nonlinear formulation needed to treat adequately this effect results in an increased analytical complexity which vitiates the attempt here to derive

simple formulae for prediction of ion implantation distributions. On the other hand, the simplified results lend themselves to reinterpretation in the presence of the nonlinear effect. Approximations of second order importance are the neglect of entrapped ion diffusion and channeling of the bombardment ion along low (Miller) index directions in the lattice. There is significant experimental evidence that diffusion is unimportant for target temperatures below 1000°C.[3] However, Bartholomew and LaPadula[12] have interpreted their experimental ion implantation data as a diffusion process, but as pointed out by Kay,[15] this is the only experimental evidence in which diffusion is considered to be a significant effect. With regard to channeling, there is ample evidence that less than a few per cent of bombardment ions are channeled in a polycrystalline target.[7]

Analysis and Results

Let $p(x)dx$ be the probability that the bombarding ion is deposited between x and $x + dx$ where x is the distance into the lattice from the surface. The function, $p(x)$, is proportional to the distribution of ions in a lightly bombarded lattice where sputtering, radiation damage, and ion-ion collisions can be neglected. Such distributions have been measured for a limited number of ion target combinations by J. A. Davies.[7] A few of these combinations have been successfully simulated by Robinson and Oen[8, 9] using numerical techniques. A more versatile, but more approximate, analytical treatment of this problem has been reported by Lindhard and Scharff.[17] As a result of their work, which is in reasonable agreement with the experimental evidence, the probability density distribution for most feasible combinations of ion, ion energy, and target lattice can be predicted.

A second parameter necessary in the calculation of the saturated ion distribution is the sputtering yield coefficient, V, which we define as the volume of solid removed per incident ion. The sputtering yield has been measured using a variety of techniques for a large number of ion-target combinations.[15] Hence, a reasonable estimate of the sputtering yield can be made by extrapolation of the data in the published literature.

If the sputtering yield and probability density distributions are known, the distribution of ions I(x, t) can be calculated for combined implantation and sputtering where the effects of ion-ion collision and ion diffusion in a damaged lattice are neglected. Equation (1) describes the continuous addition of the ion distribution to a constantly sputtered and thereby receding surface.

$$I(x, t) = j \int_0^t dt' \; p(x - jt'V) \tag{1}$$

where j is the ion current density, and t is the time. I(x, t) is taken as zero for $x < jtV$. This equation can be made more tractable by defining a new variable $\zeta = x - jtV$ as a measure of the depth into the solid from the fresh surface. Substitution then yields

$$I(\zeta, t) = \frac{1}{V} \int_{\zeta}^{\zeta + jtV} d\zeta' \; p(\zeta') \tag{2}$$

The total number of ions implanted per square centimeter I_T is obtained by integrating $I(\zeta, t)$ from the fresh surface to infinite depth.

$$I_T(t) = \frac{1}{V} \int_0^{\infty} d\zeta \int_{\zeta}^{\zeta + jtV} d\zeta' \; p(\zeta') \tag{3}$$

The condition for saturation is found by differentiating Eq (2) with

respect to time.

$$\frac{\partial I}{\partial t}(\zeta, t) = j\, p(\zeta + jtV) \tag{4}$$

The quantity $\frac{\partial I}{\partial t}$ can equal zero only when the argument of p(x) is greater than some distance ℓ for which the original distribution is essentially zero. Hence, saturation is given by the requirement that $jtV > \ell$, or, in physical terms, saturation is attained whenever the initial ion density distribution has been essentially removed by the sputtering process. This is not in agreement with the interpretation of Brown and Davies[10] who concluded that the ion distribution would approach saturation after sputtering erosion to a depth equal to the most probable penetration range.

The distribution and the areal ion density at saturation is then obtained from Eqs (2) and (3) by setting the upper limit of the integral equal to infinity.

$$I_\infty(\zeta) = I(\zeta, \infty) = \frac{1}{V}\int_{\zeta}^{\infty} d\zeta'\, p(\zeta) \tag{5}$$

$$I_{T\infty} = I_T(\infty) = \frac{1}{V}\int_{0}^{\infty} d\zeta \int_{\zeta}^{\infty} d\zeta'\, p(\zeta') \tag{6}$$

It is immediately seen that the concentration of implanted ions is inversely proportional to the sputtering yield, which is in direct agreement with the extensive experimental work of Almen and Bruce.[11] Since $p(\zeta)$ is a non negative function, the saturated ion density distribution $I_\infty(\zeta)$ is a monotonically decreasing function of depth. It should be noted that the integral in Eq (5) is equal to the f function used by Davies[7] in reporting light bombardment penetration data. Conversely, the original probability density distribution $p(\zeta)$ can be computed from the saturated condition shown in

Eq (5) by differentiating $I(\xi)$ with respect ξ .

$$p(\xi) = V \frac{dI_\infty}{d\xi} (\xi) \tag{7}$$

Eq (7) offers a convenient method for comparing the probability density distributions encountered by bombardment ions in fully damaged and in undamaged lattices; thereby allowing an experimental measure of the inaccuracy associated with the neglect of nonlinear ion-ion effects.

In order to obtain explicit predictions for I_∞ and $I_{T\infty}$, a specific functional form of p(x) must be chosen. The work of Lindhard and Scharff[17] suggests that the function should be a gaussian distribution where the mean range R and straggling σ are determined by

$$R = 3.06\left(\frac{4\pi\epsilon_o E}{Z_1 Z_2 e^2}\right)\left(\frac{1+\mu}{1+\mu/3}\right)\frac{4\pi}{aN} \tag{8}$$

and

$$\frac{R^2}{2\sigma^2} = \frac{3(1+\mu)}{(1+\mu/3)} \tag{9}$$

We define μ as the ratio of ion to target atom mass, E the ion energy, N the target atomic density, and a the Bohr screening distance taken equal to $.592\left[Z_1^{2/3} + Z_2^{2/3}\right]^{-1/2}$ (Å).

$$p(x) = \frac{1}{\sqrt{2\pi}\sigma} \exp\left\{-(x-R)^2/2\sigma^2\right\} \tag{10}$$

Substitution of Eq (10) into Eqs (5) yields

$$I_\infty (\xi \leq R) = \frac{1}{2V}\left[1 + \operatorname{erf}\left(\frac{R-\xi}{\sqrt{2}\sigma}\right)\right]$$

$$I_\infty (\xi \geq R) = \frac{1}{2V} \operatorname{erfc}\left(\frac{\xi - R}{\sqrt{2}\sigma}\right) \tag{11}$$

The areal density F of ions remaining in the lattice following uniform erosion of depth D is determined by integrating Eq (11).

$$D \leqslant R$$

$$\frac{VF}{\sqrt{2\sigma}} = \frac{R-D}{\sqrt{2\sigma}} + .564 - \frac{i^1 erfc}{2}\left(\frac{R-D}{\sqrt{2\sigma}}\right)$$

$$D \geqslant R \qquad (12$$

$$\frac{VF}{\sqrt{2\sigma}} = \frac{i^1 erfc}{2}\left(\frac{D-R}{\sqrt{2\sigma}}\right)$$

where $i^1 erfc\ (\zeta) = \int_{\zeta}^{\infty} d\zeta\ \ erfc\ \zeta$. (18)

The dimensionless group $VF/\sqrt{2\sigma}$ is plotted in Fig. 8 where it can be seen that the result can be closely approximated by

$$\frac{VF(D)}{\sqrt{2\sigma}} = \frac{R-D}{\sqrt{2\sigma}} + .564 \qquad (13$$

Hence, under uniform erosion conditions, the radioactivity of the surface can be linearly related to the depth of erosion.

The total areal density $I_{T\infty}$ for a gaussian probability function is determined from Eq (12) by setting D = 0.

$$I_{T\infty} = \frac{\sqrt{2\sigma}}{V}\left[.564 + (R/\sqrt{2\sigma}) - 1/2\ \ i^1 erfc\ (R/\sqrt{2\sigma})\right] \qquad (14$$

A plot of this equation, using dimensionless grouping of parameters, is presented in Fig. 9. Two limiting cases are of interest:

$$\lim_{(R/\sqrt{2\sigma}) \to \infty} I_{T\infty} = R/V \qquad (15$$

$$\lim_{(R/\sqrt{2\sigma}) \to 0} I_{T\infty} = .4\sigma/V \qquad (16$$

In most applications of tracer ion implantation, the depth of penetration R is large in comparison to the straggling. Under this condition, Eq (15) is applicable, and the total areal density can be taken as proportional to the range and inversely proportional to the sputtering yield. It would seem that this limiting case offers a useful rule of thumb in estimating the total tracer ion activity that can be implanted without recourse to simultaneous surface replenishment.

A sample calculation of ion implantation using 40 keV argon bombardment of tungsten yields a total areal density of 4.3×10^{16} cm^{-2}; the sputtering yield is taken from the data of Almen and Bruce[11] as 2.3 atoms/ion, and the unsaturated ion distribution has been measured by Kornelson.[7] In this particular case, the non-linear effect of ion-ion collisions is important, but it would seem that the limiting situation shown in Eq (15) can be applied in the sense that $I_{T\infty}$ will be less than the above calculation since the most probable distance of penetration, R. is reduced as a result of ion-ion collisions in the lattice.

For most applications of ion implantation it is desirable to maximize $I_{T\infty}$. If this is the case, the desired result can be best obtained by using as high an ion energy as possible since the range of the ion increases linearly with energy whereas the sputtering yield remains constant or decreases for energies above 10 keV. Similarly, for those ion target combinations where $R/\sqrt{2}\sigma$ is small (i. e. those cases for which Eq (16) is applicable) high energy bombardment again maximizes the areal concentration of ions since the straggling σ can be taken as proportional to the ion energy and again the sputtering yield decreases for energies above 10 keV. Clearly, the target material should have as low a sputtering yield as possible.

In summary, it has been the purpose of this note to present a simplified analysis of the combined effects of ion implantation and sputtering amenable to quick and relatively accurate calculation of the absolute ion distribution in the lattice at saturation.

REFERENCES:

1. N. Thomas Olson and Harold P. Smith, Jr., "Measurement of Cesium Sputtered Copper Yield and Angular Distribution by a Radioactive Tracer Technique," AIAA Paper No. 65-379.

2. Harold P. Smith, Jr., and F. C. Hurlbut, "Quarterly Progress Report: Investigation of Kilovolt Ion Sputtering," NASA CR-54406.

3. D. E. Harrison, Jr., private communication.

4. C. H. Townes, Phys. Rev., 65, 319 (1944).

5. Henke, White, and Lundberg, "Semiemperical Determination of Mass Absorption Coefficients for the 5 to 50 Angstrom X-ray Region," J. Appl. Phys., 28, 98 (1957).

6. L. Harris, "Preparation and Infra-red Properties of Aluminum Oxide Films," J. Optical Society of America, 45, 27 (1955).

7. Kornelson, E. V., Brown, F., Davies, J. A., Domeij, B., and Piercy, G. R., "Penetration of Heavy Ions of KeV Energies into Monocrystalline Tungsten," Phys. Rev. 136A, 849-858 (1964) and earlier references noted therein.

8. M. T. Robinson and O. S. Oen, "Computer Studies of the Slowing Down of Energetic Atoms in Crystals," Phys. Rev. 132, 2385-2398 (1963).

9. O. S. Oen and M. T. Robinson, "Monte Carlo Range Calculations for a Thomas Fermi Potential," J. Appl. Phys., 35, 2515-2521 (1964).

10. F. Brown and J. A. Davies, "The Effect of Energy and Integrated Flux on the Retention and Range of Inert Gas Ions Injected at KeV Energies in Metals," Can. J. Phys. 41, 844-857 (1963).

REFERENCES (continued)

11. Almen, O., and Bruce, G., "Collection and Sputtering Experiments with Noble Gas Ions," Nucl. Instr. Methods, 11, 257-278 and 279-289, (1961).

12. Bartholomew, C. Y., and LaPadula, A. R., "Penetration of Krypton Ions into Molybdenum in a Glow Discharge," J. Appl. Phys., 35, 2570-2572 (1964).

13. Lutz, H., and Sizmann, R., "Super Ranges of Fast Ions in Copper Single Crystals," Phys. Letters, 5, 113-114 (1963).

14. Nelson, R. S., and Thompson, M. W., "The Penetration of Energetic Ions Through the Open Channels in a Crystal Lattice," Phil, Mag. 8, 1677-1690 (1963).

15. The most recent review of sputtering has been published by Kay, E., "Impact Evaporation and Thin Film Growth in a Glow Discharge," Advances in Electronics and Electron Physics 17, 245-322 (1962).

16. Carter, G., Colligon, J. S., and Leck, J. H., "Ion Sorption in the Presence of Sputtering," Proc. Phys. Soc. 79, 299 (1962).

17. Lindhard, J., and Scharff, M., "Energy Dissipation by Ions in the kev Region," Phys. Rev. 124, 128-130 (1961).

18. Abramowitz, M., and Stegun, I. A., Handbook of Mathematical Functions (National Bureau of Standards, Applied Mathematical Series 55, 1964) p. 299.

QUARTERLY REPORT DISTRIBUTION LIST

Contract NAS 3-5743

Copies	Addressee
	NASA Headquarters FOB - 10B 600 Independence Avenue, NE Washington, D. C. 20546
2	Attention: RNT/James Lazar
	NASA-Lewis Research Center 21000 Brookpark Road Cleveland, Ohio 44135
2	Attention: J. H. Childs
1	D. L. Lockwood
5	J. A. Wolters
1	Y. E. Strausser
1	J. H. DeFord
1	Tech. Utilization Office
2	Library
1	Reports Control Office
1	W. Moeckel
	Hughes Research Laboratory 3011 Malibu Canyon Road Malibu, California
1	Attn: Dr. G. Brewer
1	Dr. H. Wiser
	Electro-Optical Systems, Inc. 125 North Vinedo Avenue Pasadena, California
1	Attn: A. T. Forrester
1	Dr. D. B. Medved
	Litton Systems, Inc. Beverly Hills, California
1	Attn: Dr. G. K. Wehner
	General Dynamics/Astronautics P. O. Box 1128 San Diego, California 92112
1	Attn: Dr. D. Magnuson
	Field Emission Corporation 611 Third Street McMinnville, Oregon
1	Attn: Dr. L. W. Swanson
	General Electric Company Flight Propulsion Laboratory Evendale, Ohio
1	Attn: Dr. M. L. Bromberg

Copies	Addressee
	AFWL Kirtland Air Force Base, New Mexico
1	WLPC/Capt. C. F. Ellis
	Space Technology Laboratories One Space Park Redondo Beach, California
1	Attn: Dr. D. B. Langmuir
	NASA-Marshall Space Flight Center Huntsville, Alabama 35812
1	M-RP-DIR/E. Stuhlinger
	NASA Scientific and Technical Information Facility Box 5700 Bethesda, Maryland 20014
6	Attn: NASA Rep./RQT-2448
	Commander Aeronautical Systems Division Wright-Patterson Air Force Base, Ohio
1	WPAFP-AFAPL (APIE)/Robert Supp
	NASA-Ames Research Center Moffett Field, California 94035
1	Attn: T. W. Snouse
	Varian Associates 611 Hansen Way Palo Alto, California
1	Attn: Technical Library
	Astro-Met Associates, Inc. 500 Glendale-Milford Road Cincinnati, Ohio 45215
1	Attn: J. W. Graham
	Princeton University Department of Aeronautical Engineering Princeton, New Jersey
1	Attn: Professor J. B. Venn
	Hiram College Department of Physics Hiram, Ohio
1	Attn: Professor L. Shaffer
	University of Missouri Materials Research Center Rolla, Missouri
1	Attn: J. R. Wolfe

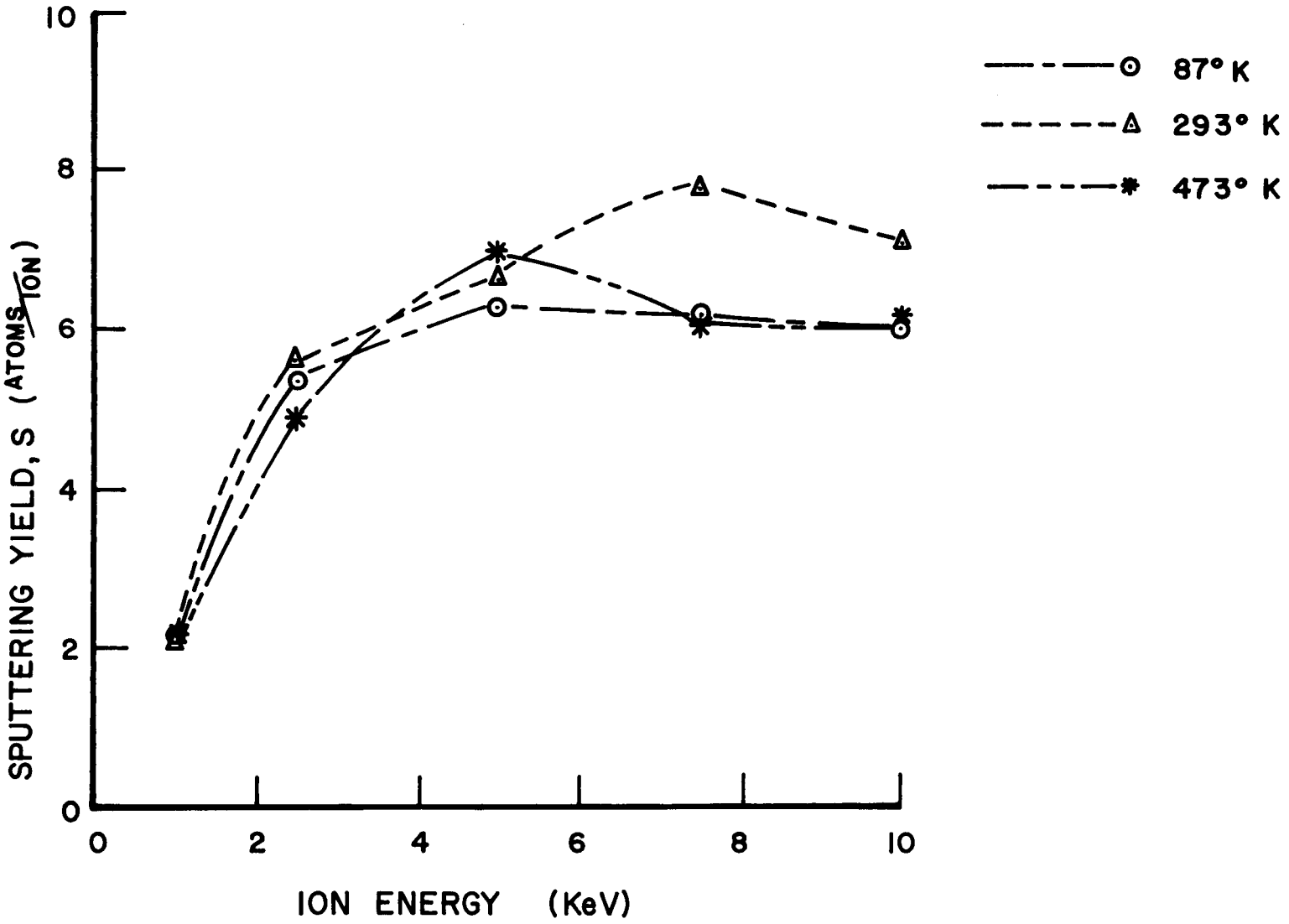

Fig. 1. Sputtering yield versus incident ion energy for 1 - 10 KeV cesium ion bombardment of monocrystalline copper at 87°K., 293°K., and 473°K. The ion beam was normal to the surface and parallel to the < 100 > direction.

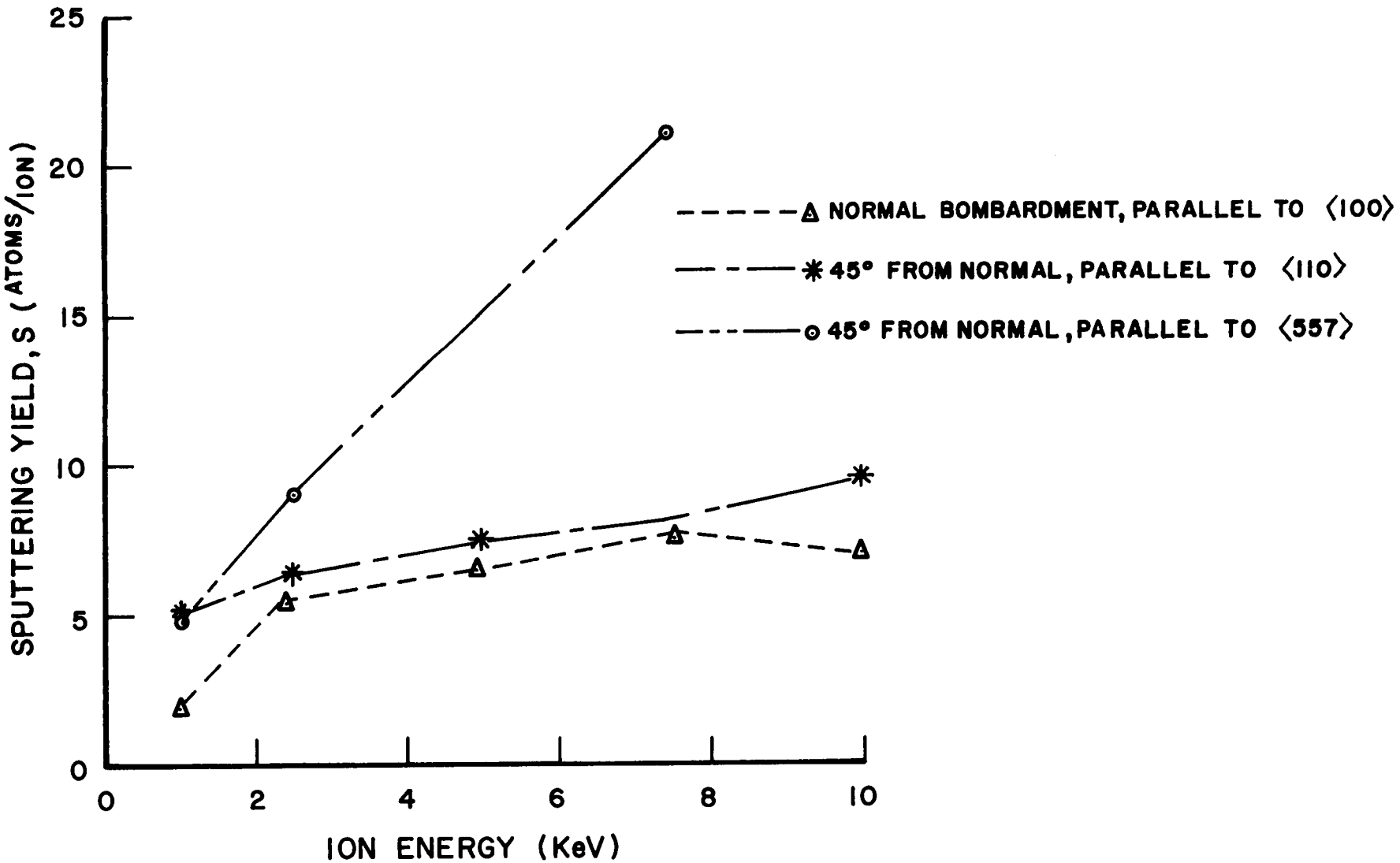

Fig. 2. Sputtering yield versus incident ion energy for 1 - 10 KeV cesium ion bombardment of monocrystalline copper at 293°K. The ion beam was 45° from the surface normal and parallel to the ⟨110⟩ or ⟨557⟩ crystallographic direction as indicated.

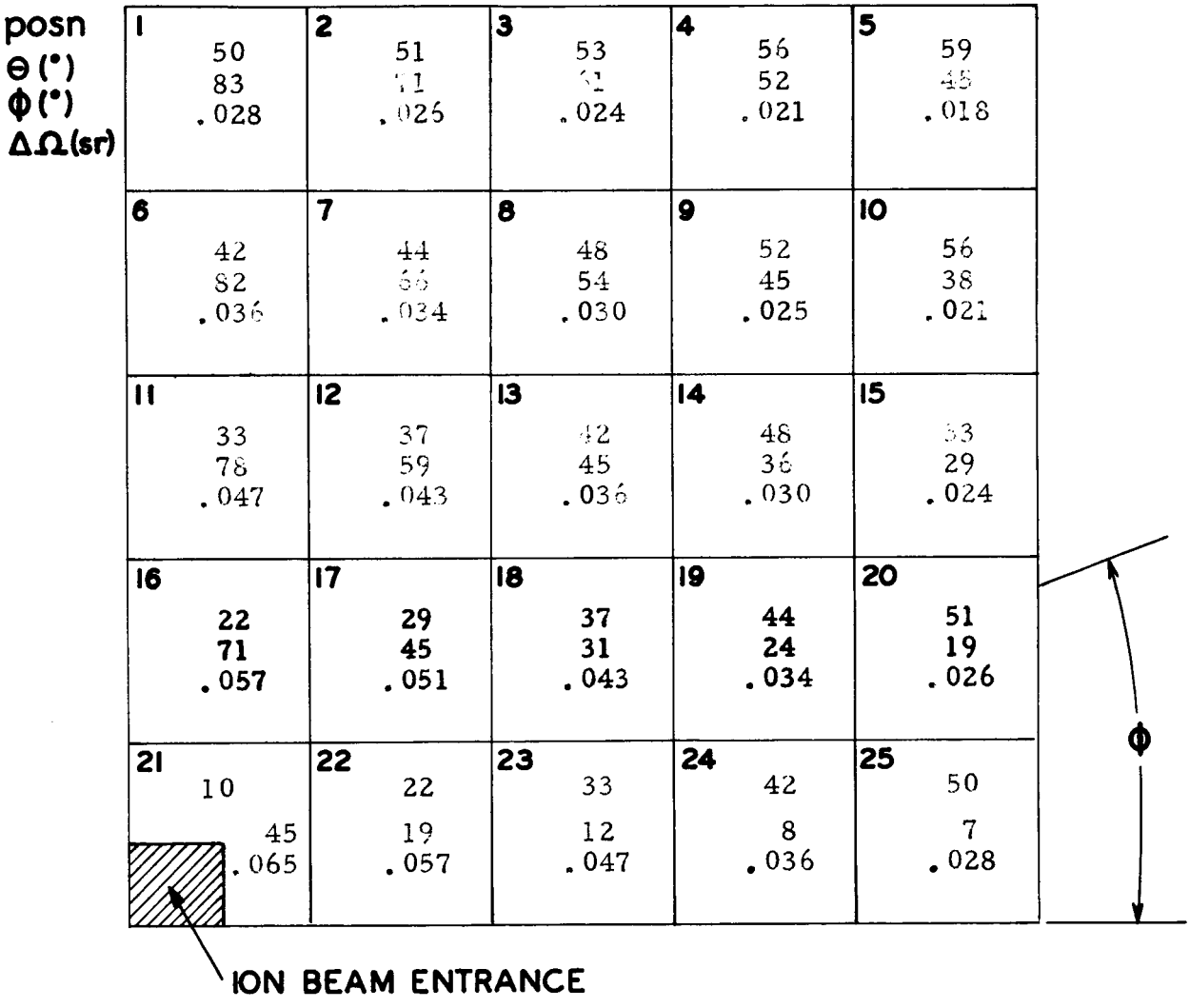

Fig. 3. Schematic diagram of the angular collector positions for normal bombardment of the (100) surface. Θ is the polar angle taken equal to zero along the surface normal while ϕ is the azimuthal angle measured as shown in the surface plane. The solid angle in sterradians is presented for each collector position.

POSITION θ (°) Φ (°) ΔΩ (Sr)									
1 59 135 .018	2 56 128 .021	3 53 119 .024	4 51 109 .026	5 50 97 .028	6 50 83 .028	7 51 71 .026	8 53 61 .024	9 56 52 .021	10 59 45 .018
11 56 142 .021	12 52 135 .025	13 48 126 .030	14 44 114 .034	15 42 98 .036	16 42 82 .036	17 44 66 .034	18 48 54 .030	19 52 45 .025	20 56 38 .021
21 53 151 .024	22 48 144 .030	23 42 135 .036	24 37 121 .043	25 33 102 .047	26 33 78 .047	27 37 59 .043	28 42 45 .036	29 48 36 .030	30 53 29 .024
31 51 161 .026	32 44 156 .034	33 37 149 .043	34 29 135 .051	35 22 109 .057	36 22 71 .057	37 29 45 .051	38 37 31 .043	39 44 24 .034	40 51 19 .026
41 50 173 .028	42 42 172 .036	43 33 168 .047	44 22 161 .057	45 10 135 .065	46 10 45 .065	47 22 19 .057	48 33 12 .047	49 42 8 .036	50 50 7 .028
51 50 187 .028	52 42 188 .036	53 33 192 .047	54 22 199 .057	55 10 225 .065	56 10 315 .065	57 22 341 .057	58 33 348 .047	59 42 352 .036	60 50 353 .028
61 51 199 .026	62 44 204 .034	63 37 211 .043	64 29 225 .051	65 22 251 .057	66 22 289 .057	67 29 315 .051	68 37 329 .043	69 44 336 .034	70 51 351 .026
71 53 209 .024	72 48 216 .030	73 42 225 .036	74 37 239 .043	75 33 258 .047	76 33 382 .047	77 37 301 .043	78 42 315 .036	79 48 324 .030	80 53 331 .024
81 56 218 .021	82 52 225 .025	83 48 234 .030	84 44 246 .034	85 42 262 .036	86 42 278 .036	87 44 294 .034	88 48 306 .030	89 52 315 .025	90 56 322 .021
91 59 225 .018	92 56 232 .021	93 53 241 .024	94 51 261 .026	95 50 263 .028	96 50 277 .028	97 51 289 .026	98 53 299 .024	99 56 308 .021	100 59 315 .018

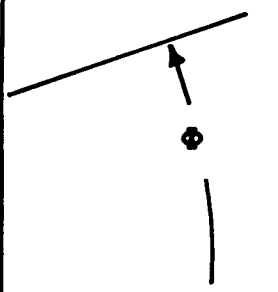

ION BEAM ENTRANCE

Fig. 4. Schematic diagram of the angular collector positions for non-normal bombardment of the surface. All 100 collector positions are shown since the previous symmetry conditions do not exist for non-normal bombardment. θ is the polar angle taken equal to zero along the surface normal (black dot in center) while ϕ is the azimuthal angle measured about the surface normal in the plane parallel to the surface.

ION ENERGY - 1 kv
ANGLE OF INCIDENCE - 45° ALONG <110>

2.30	2.37	2.30	1.63	1.20	1.06	1.29	1.16	0.94	0.57
2.69	3.63	3.47	2.62	1.83	1.34	1.32	2.16	1.97	1.03
2.74	4.30	4.80	3.62	2.58	2.30	1.95	2.47	2.03	1.31
2.29	2.65	4.05	3.16	2.27	2.20	1.86	1.90	1.17	0.81
1.09	2.01	2.75	2.43	1.73	1.64	1.32	1.30	0.87	0.25
1.15	1.24	1.82	1.84	1.48	1.21	1.00	0.71	0.66	0.18
1.29	1.27	2.00	1.64	1.14	1.09	0.75	1.06	0.67	0.62
1.39	2.06	2.17	2.04	1.25	0.91	0.82	1.06	1.03	0.40
1.44	2.25	2.36	1.10	0.94	0.85	0.87	0.72	0.60	0.25
1.72	1.60	1.61	0.80	0.60	0.38	0.57	0.56	0.29	0.69

Fig. 5A. Angular distribution normalized to isotropic emission for cesium ion sputtering of monocrystalline copper. The 1.0 KeV ion beam was 45 degrees from the surface normal and parallel to the ⟨110⟩ vector. The angular position of each point is depicted in Fig. 4.

ION ENERGY - 2.5^{kv}
ANGLE OF INCIDENCE - 45° ALONG <110>

2.29	2.06	2.41	1.68	1.34	1.30	0.97	1.15	0.82	1.16
1.77	4.25	3.19	2.49	1.67	1.63	1.48	2.08	2.63	1.25
1.58	3.17	4.23	2.78	2.39	2.32	2.59	2.50	2.15	1.52
1.19	1.42	2.98	2.16	2.21	2.00	1.96	1.97	1.03	0.83
1.07	1.63	2.10	2.10	1.88	1.82	1.76	1.48	0.91	0.93
0.83	1.17	2.01	1.83	1.72	1.66	1.42	1.21	1.07	1.01
1.22	1.70	1.88	1.61	1.43	1.33	1.02	1.34	0.91	0.35
0.64	1.41	1.84	1.84	1.54	1.05	1.16	1.33	1.60	0.71
1.49	2.53	1.93	1.29	1.15	0.85	0.95	1.37	2.21	0.47
1.15	1.45	1.30	0.74	0.45	0.41	0.91	0.79	1.09	0.88

Fig. 5B. Angular distribution normalized to isotropic emission for cesium ion sputtering of monocrystalline copper. The 2.5 KeV ion beam was 45 degrees from the surface normal and parallel to the <110> vector. The angular position of each point is depicted in Fig. 4.

ION ENERGY - 5 kv
ANGLE OF INCIDENCE - 45° ALONG <110>

1.50	2.14	1.81	1.54	1.26	1.05	1.12	0.96	0.69	0.85
1.20	2.97	4.58	1.76	1.51	1.58	1.42	1.77	1.99	1.65
1.42	2.23	5.96	4.38	2.08	2.07	1.70	2.33	2.30	1.47
1.21	1.64	2.23	2.35	1.91	1.65	1.91	2.39	1.97	1.14
0.91	1.19	1.74	1.80	1.58	1.62	1.53	1.67	1.15	1.10
1.19	1.47	1.77	1.60	1.55	1.81	1.53	1.24	1.25	0.58
0.43	1.29	1.77	1.66	1.55	1.18	1.34	1.17	0.96	0.39
1.23	1.69	1.77	1.96	1.14	1.26	1.37	1.84	1.69	0.76
1.42	1.95	2.19	1.61	1.12	1.03	1.31	1.41	1.76	0.86
1.50	1.23	1.41	1.20	0.80	0.67	0.72	1.34	0.94	0.94

Fig. 5C. Angular distribution normalized to isotropic emission for cesium ion sputtering of monocrystalline copper. The 5.0 KeV ion beam was 45 degrees from the surface normal and parallel to the <110> vector. The angular position of each point is depicted in Fig. 4.

ION ENERGY - 7.5 kv

ANGLE OF INCIDENCE - 45° ALONG <110>

0.93	1.92	1.98	1.44	1.14	0.91	0.84	0.94	0.98	1.00
1.33	2.84	3.92	1.59	1.19	1.06	1.32	1.49	1.48	1.35
1.10	2.35	2.68	2.55	1.85	1.51	1.73	2.23	2.54	1.44
1.05	1.58	1.96	2.01	1.87	1.76	1.96	1.85	1.40	1.44
0.76	1.04	1.81	1.78	1.88	1.74	1.76	1.55	1.49	0.97
0.99	1.12	1.37	1.82	1.80	2.19	1.65	1.64	1.09	0.68
0.76	1.61	1.83	1.83	1.80	1.69	1.73	1.69	1.24	0.70
1.16	1.52	2.22	2.07	1.71	1.22	1.55	2.42	1.51	0.99
1.67	2.82	2.39	1.53	1.14	1.32	1.41	1.89	2.13	1.47
1.19	1.46	1.87	1.34	0.91	0.78	1.07	1.32	1.45	1.80

Fig. 5D. Angular distribution normalized to isotropic emission for cesium ion sputtering of monocrystalline copper. The 7.5 KeV ion beam was 45 degrees from the surface normal and parallel to the <110> vector. The angular position of each point is depicted in Fig. 4.

ION ENERGY - 10^{kv}
ANGLE OF INCIDENCE - 45° ALONG <110>

0.79	1.45	0.22	1.04	1.05	0.80	0.92	1.12	0.82	1.04
2.23	2.27	1.75	1.56	1.43	1.71	1.74	1.73	1.83	1.83
1.33	2.48	2.79	2.51	1.75	1.71	2.27	2.31	2.29	1.62
1.88	1.88	1.99	2.63	2.21	1.72	2.45	2.25	1.60	1.38
1.06	1.37	1.82	1.76	1.88	2.08	1.90	1.98	1.05	0.86
1.10	1.55	1.69	1.79	2.08	2.44	1.63	1.25	1.29	0.65
0.95	1.73	1.38	1.83	1.63	1.78	1.83	1.29	1.06	0.47
0.74	1.36	2.04	1.84	1.45	1.49	1.41	1.24	1.60	1.27
1.02	1.56	1.51	2.06	1.40	1.75	1.30	0.96	2.03	1.28
0.94	0.90	1.63	0.95	0.86	0.93	1.48	0	1.93	0.36

Fig. 5E. Angular distribution normalized to isotropic emission for cesium ion sputtering of monocrystalline copper. The 10.0 KeV ion beam was 45 degrees from the surface normal and parallel to the <110> vector. The angular position of each point is depicted in Fig. 4.

ION ENERGY - 1 kv

ANGLE OF INCIDENCE - 45° ALONG <557>

0.93	0.95	1.29	2.27	3.33	3.65	2.37	1.52	0.82	1.00
0.74	1.01	1.42	2.29	3.12	3.36	2.26	1.13	0.73	0.77
1.22	1.44	2.04	2.32	2.53	2.57	1.76	1.31	1.05	0.79
2.20	2.26	2.55	2.42	1.88	1.86	1.61	1.28	1.22	1.07
3.10	3.60	2.68	2.11	1.65	1.50	1.43	1.41	1.43	1.18
2.83	3.00	2.58	1.90	1.40	1.27	1.11	1.22	1.34	1.32
1.32	1.57	1.90	1.61	1.30	1.07	1.00	0.60	0.57	0.67
0.98	1.13	1.13	1.18	1.34	1.15	0.74	0.79	0.61	0.16
0.54	0.73	0.83	0.94	1.22	1.27	0.70	0.38	0.61	0.18
0.51	0.62	0.75	0.60	1.15	0.99	0.45	0.36	0.53	0

Fig. 6A. Angular distribution normalized to isotropic emission for cesium ion sputtering of monocrystalline copper. The 1.0 KeV ion beam was 45 degrees from the surface normal and parallel to the <557> vector. The angular position of each point is depicted in Fig. 4.

ION ENERGY - 2.5 kv
ANGLE OF INCIDENCE - 45° ALONG <557>

1.07	1.09	1.51	1.81	2.61	3.26	2.31	1.28	0.90	0.36
0.68	1.65	1.53	1.79	4.02	2.83	1.82	1.40	1.03	0.87
1.04	1.32	1.93	2.01	2.31	2.35	1.91	1.81	1.10	1.07
1.71	1.99	2.03	2.17	2.27	2.16	1.82	1.56	1.86	1.56
2.10	2.66	2.21	2.02	1.82	2.19	1.88	1.59	1.97	2.28
2.05	1.79	2.06	1.68	1.76	1.72	1.55	1.40	1.41	1.03
0.95	1.05	1.16	1.39	1.19	1.33	1.01	0.89	1.05	0.27
0.62	0.60	0.88	1.13	1.42	1.53	1.12	0.69	0.65	0.48
0.56	0.65	0.49	1.04	1.22	1.68	1.07	0.63	0.42	0.28
0.59	0.40	0.63	0.93	0.94	1.24	0.85	0.54	0.10	0.22

Fig. 6B. Angular distribution normalized to isotropic emission for cesium ion sputtering of monocrystalline copper. The 2.5 KeV ion beam was 45 degrees from the surface normal and parallel to the <557> vector. The angular position of each point is depicted in Fig. 4.

ION ENERGY - 7.5 kv
ANGLE OF INCIDENCE - 45° ALONG <557>

0.90	0.69	1.03	1.35	2.25	2.65	1.83	1.04	0.70	0.80
0.88	1.11	1.26	1.47	3.15	2.23	1.70	1.26	0.90	0.67
1.01	1.16	1.49	1.81	2.03	2.30	1.77	1.55	1.15	0.93
1.42	1.67	1.89	1.96	2.11	2.08	1.82	1.62	1.53	1.36
2.28	2.34	2.09	2.11	2.29	2.51	1.88	1.93	2.17	2.04
2.22	2.35	2.15	1.95	2.19	2.39	1.91	1.78	1.87	2.07
1.18	1.36	1.63	1.75	1.85	1.90	1.63	1.35	1.04	0.95
0.81	0.87	1.05	1.49	1.92	1.86	1.40	0.66	0.54	0.61
0.63	0.68	0.89	1.09	1.88	2.22	1.23	0.62	0.60	0.39
0.64	0.68	0.67	0.85	1.34	1.78	1.11	0.59	0.45	0.30

Fig. 6C. Angular distribution normalized to isotropic emission for cesium ion sputtering of monocrystalline copper. The 7.5 KeV ion beam was 45 degrees from the surface normal and parallel to the <557> vector. The angular position of each point is depicted in Fig. 4.

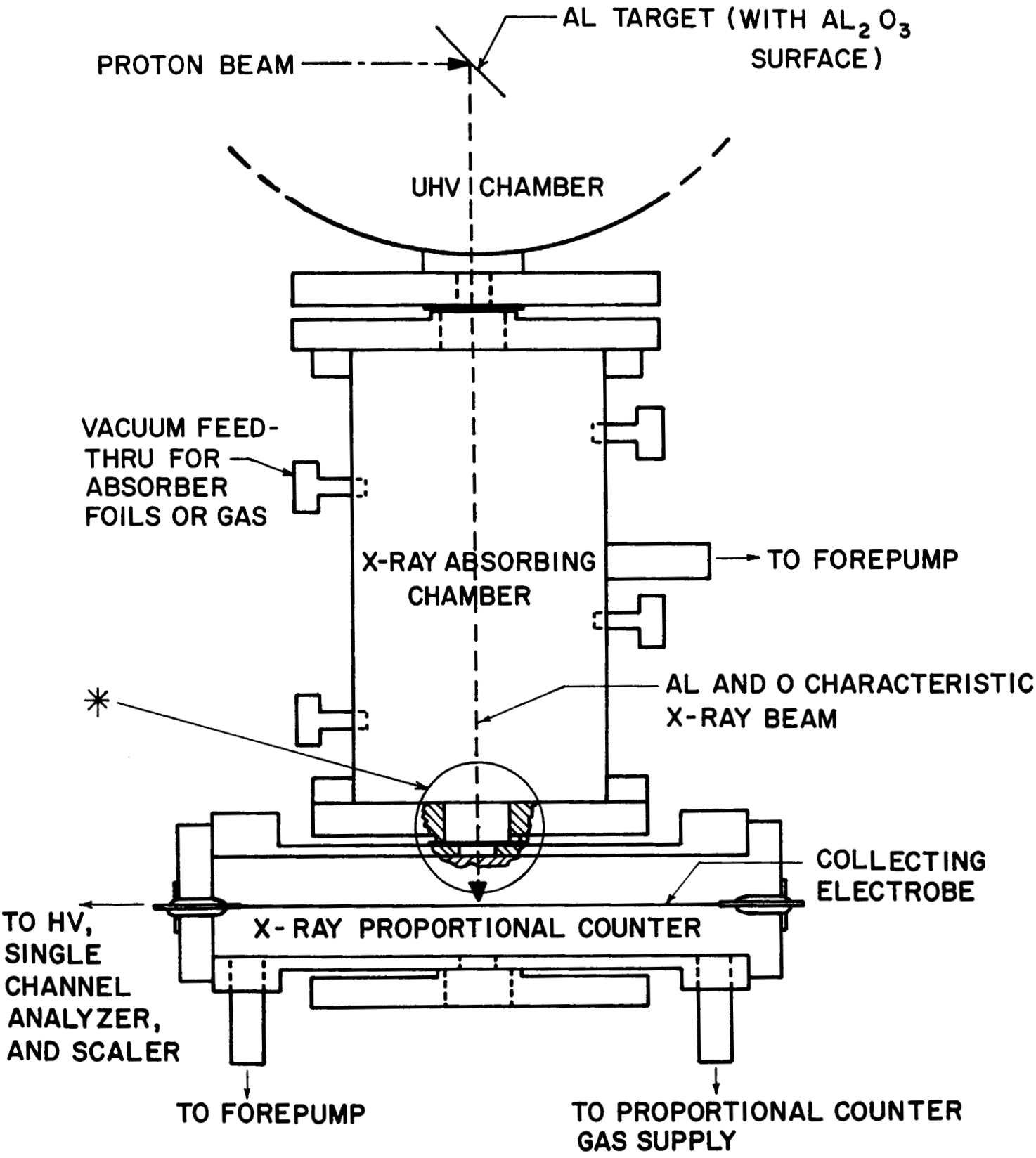

Fig. 7. Schematic diagram of proton induced characteristic x-ray detection system.

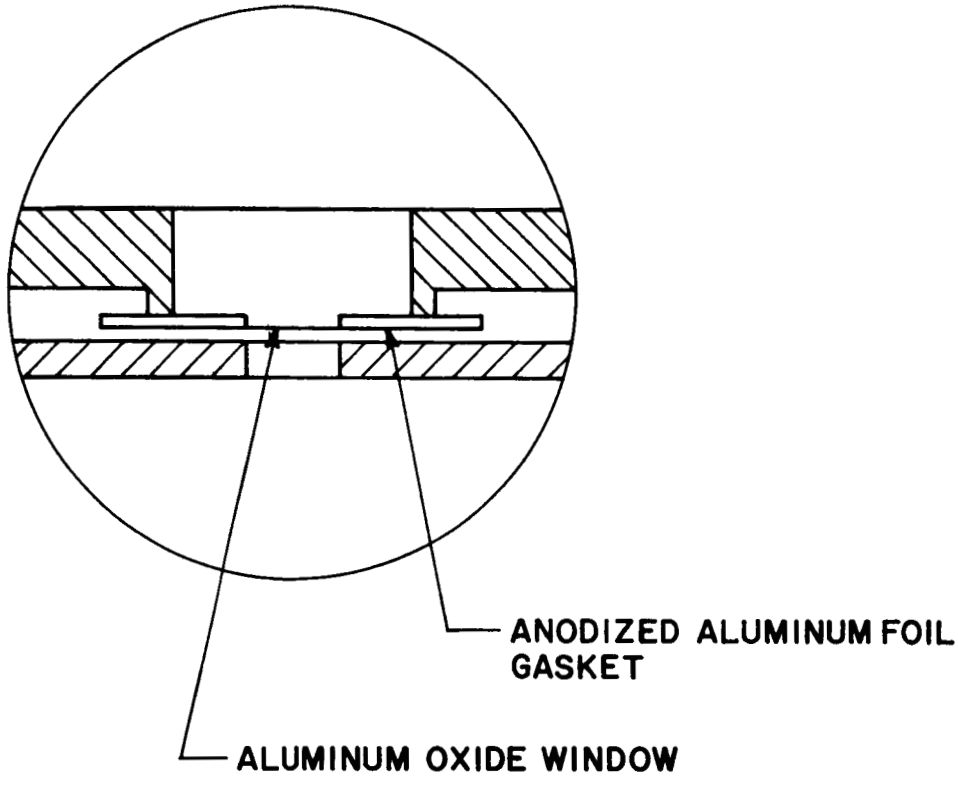

DETAIL A

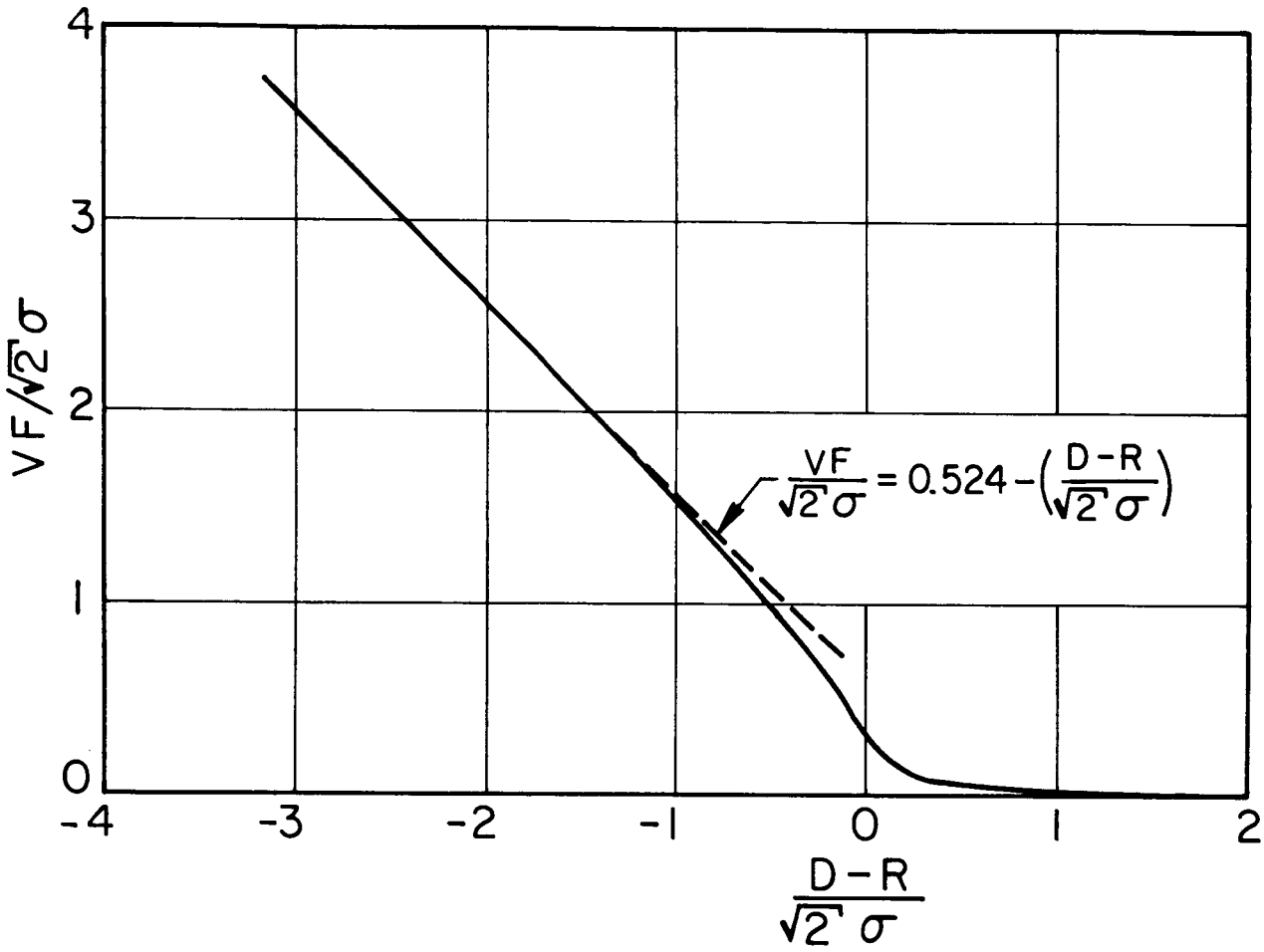

Fig. 8. Residual area density of implanted ions, F (ions/cm^2), as a function of the depth of erosion, D (cm). The parameters are plotted as dimensionless groups according to the relationship shown in Eq (12). A linear approximation to the exact solution is depicted.

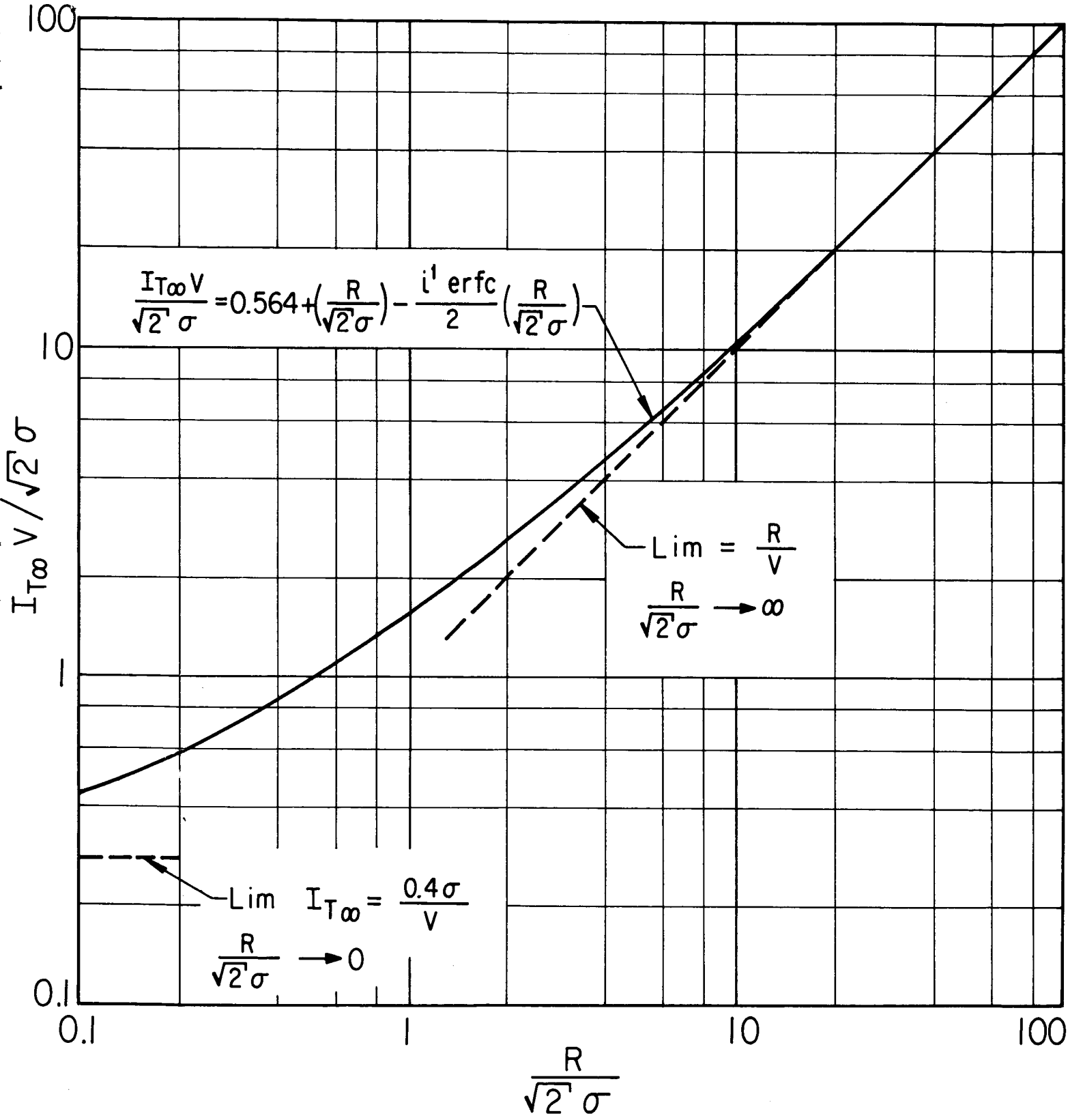

Fig. 9. Saturation areal ion density, $I_{T\infty}$ (ions/cm^2) as a function of the sputtered yield, ion penetration range, and ion straggling. The parameters are plotted as dimensionless groups according to the relationship shown in Eq (14). Two limiting cases are also depicted.

Energy (keV) ϕ(<110>)	1 67°	2.5 53°	5 45°	7.5 45°	10 23°
position			$(\Delta s/\Delta\Omega\ /s/2\pi)$		
1	1.38	1.02	0.89	0.90	1.03
2	2.61	1.53	1.05	0.93	0.92
3	2.23	2.27	1.18	0.98	0.72
4	1.06	1.78	1.26	1.23	0.73
5	0.67	1.54	1.69	1.75	0.88
6	2.06	1.38	1.28	1.33	1.42
7	2.55	2.07	1.38	1.36	1.24
8	1.97	2.72	1.92	1.86	1.05
9	0.87	2.11	2.58	2.87	1.07
10	0.37	1.09	2.19	2.30	1.23
11	2.11	1.56	1.68	1.74	1.66
12	1.98	1.98	1.72	1.83	1.66
13	1.90	2.22	2.49	2.53	1.72
14	0.98	1.56	2.81	2.93	2.23
15	0.61	0.98	1.76	1.80	2.75
16	1.57	1.39	1.61	1.67	1.71
17	1.63	1.62	1.59	1.68	1.60
18	1.58	1.71	1.89	1.97	2.01
19	1.00	1.35	1.87	1.80	2.80
20	0.72	0.88	1.06	1.10	3.05
21	1.42	1.58	1.86	1.84	2.15
22	1.38	1.45	1.56	1.65	1.62
23	1.58	1.53	1.68	1.78	1.78
24	1.29	1.29	1.37	1.49	1.94
25	0.99	0.97	1.01	0.85	1.37

Table 1. Relative angular distribution normalized to isotropic emission as a function of ion energy for normal bombardment of the (100) plane with the target temperature equal to 87°K. The angular position number corresponds to that shown in Fig. 3. Azimuthal orientation of the (010) plane which contains a <110> closepacked vector is shown for each measurement.

Energy (keV) ϕ (<110>)	1 45°	2.5 45°	5 45°	7.5 45°	10 45°
position	($\Delta s/\Delta\Omega$ / $s/2\pi$)				
1	0.83	0.96	0.86	0.97	0.93
2	0.97	1.17	1.10	1.09	1.01
3	1.36	1.47	1.25	1.38	1.19
4	1.71	1.83	1.53	1.63	1.55
5	1.63	1.71	1.56	1.68	1.54
6	1.31	1.18	1.37	1.34	1.33
7	1.59	1.69	1.56	1.55	1.39
8	2.17	2.15	2.05	2.08	2.02
9	2.83	2.52	2.56	2.26	2.33
10	1.81	1.59	1.58	1.53	1.53
11	1.66	1.76	1.95	1.74	1.88
12	2.05	2.08	2.06	2.00	2.10
13	2.79	2.50	2.62	2.35	2.54
14	2.18	2.10	2.21	1.99	2.30
15	1.56	1.30	1.52	1.30	1.46
16	1.56	1.64	1.85	1.80	1.90
17	1.85	1.77	1.89	1.74	1.96
18	2.04	1.96	2.11	1.86	2.10
19	1.69	1.56	1.73	1.46	1.56
20	1.11	1.13	1.08	1.08	0.99
21	1.64	1.82	2.31	2.28	2.47
22	1.54	1.63	1.89	1.75	1.86
23	1.68	1.78	1.59	1.69	1.87
24	1.40	1.44	1.50	1.34	1.35
25	0.91	0.84	0.97	0.92	0.93

Table 2. Relative angular distribution at 473°K. The bombardment conditions and configuration are analogous to those presented in Table 1.